Univerzita Komenského v Bratislave
Fakulta matematiky, fyziky a informatiky

Mgr. Ľuboš Bičian

Autoreferát dizertačnej práce

Measurement of $K^+ \to \pi^+\mu^+\mu^-$ Decay Form Factor and Evaluation of Muon Veto and Charged Hodoscope Efficiencies at NA62 Experiment at CERN

na získanie akademického titulu *philosophiae doctor*
v odbore doktorandského štúdia: 4.1.5. Jadrová a subjadrová fyzika

BRATISLAVA, 2019

Dizertačná práca bola vypracovaná v dennej forme doktorandského štúdia na
Katedre teoretickej fyziky
Fakulty matematiky, fyziky a informatiky
Univerzity Komenského v Bratislave.

Predkladateľ: Mgr. Ľuboš Bičian
Katedra teoretickej fyziky
Fakulta, matematiky, fyziky a informatiky
Univerzity Komenského
Mlynská dolina
842 48 Bratislava

Školiteľ: doc. RNDr. Vladimír Černý, CSc.
Katedra teoretickej fyziky
FMFI UK Bratislava

Oponenti:

Obhajoba dizertačnej práce sa koná dňa ..... o ..... h pred komisiou pre obhajobu dizertačnej práce v odbore doktorandského štúdia vymenovanou predsedom odborovej komisie dňa ..... .

4.1.5. Jadrová a subjadrová fyzika

Predseda odborovej komisie:

prof. RNDr. Jozef Masarik, DrSc.
Katedra jadrovej fyziky a biofyziky
Fakulta, matematiky, fyziky a informatiky
Univerzity Komenského
Mlynská dolina
842 48 Bratislava

Abstract

NA62 is a cutting-edge kaon experiment located at CERN, focusing primarily on rare decays of positively charged kaons in flight.

The main focus of the presented thesis is the measurement of form factor parameters and the branching fraction of a rare kaon decay $K^+ \to \pi^+\mu^+\mu^-$ ($K_{\pi\mu\mu}$) at the NA62 experiment, using a sub-sample of data collected in 2017. Therefore, a motivation for the measurement, a summary of the theoretical description within the scope of the Chiral Perturbation Theory and a review of the previous measurements of the $K_{\pi\mu\mu}$ decay parameters are given.

The central part of the work contains detailed description of the main $K_{\pi\mu\mu}$ analysis done by the author, together with the derivation and validation of the fitting procedure used to obtain the $K_{\pi\mu\mu}$ form factor parameters. Based on the sample of 3074 observed $K_{\pi\mu\mu}$ event candidates in the dataset, we obtain form factor parameter values $a = -0.564 \pm 0.042$ and $b = -0.797 \pm 0.164$, which gives a model-dependent branching fraction $\mathcal{B}(K_{\pi\mu\mu}) = (9.32 \pm 0.29) \times 10^{-8}$, consistent with the previous measurements.

Low background contamination of the selected signal sample makes the contribution from statistical errors smaller by $\approx$ 10–20% with respect to the currently most precise $K_{\pi\mu\mu}$ measurement performed by the NA48/2 experiment, which collected similar number of $K_{\pi\mu\mu}$ event candidates but with $\approx 3\%$ background contamination.

However, the total systematic uncertainty is of a similar size as the statistical one, which makes the precision of the presented result worse by $\approx$ 10–20% compared to the NA48/2 result. Improvement of systematic uncertainties is crucial for achieving the world-leading measurement in the future, particularly when the full available NA62 dataset, expected to contain at least 5-times more $K_{\pi\mu\mu}$ event candidates than the NA48/2 dataset, is analysed.

In addition to the main $K_{\pi\mu\mu}$ analysis, efficiency evaluation studies for sub-detectors MUV3 and CHOD carried out by the author are summarised in the thesis. The measured efficiencies were monitored during the NA62 data taking in 2016–2018 using the developed tools. Their values were stable over the period and above 99%. The results of MUV3 efficiency measurements are also used in the main $K_{\pi\mu\mu}$ analysis.

The main goal of the NA62 experiment is the measurement of the branching fraction of an ultra-rare $K^+ \to \pi^+\nu\bar{\nu}$ ($K_{\pi\nu\nu}$) decay, sometimes referred to as the "golden decay" due to the fact that it is theoretically very clean and sensitive to contributions of New Physics. These properties make the $K_{\pi\nu\nu}$ decay an excellent probe of the physics beyond the Standard Model. The measurement of the $K_{\pi\nu\nu}$ decay branching fraction is discussed in the thesis and the first result of the analysis performed on the 2016 data sample is summarised.

Keywords: NA62 experiment, rare kaon decays, charged kaon form factor

Abstrakt

Experiment NA62 je špičkovým kaónovým experimentom nachádzajúcim sa v CERN-e, zameraným na štúdium zriedkavých rozpadov nabitých kaónov za letu.

Hlavným cieľom práce je meranie parametrov form-faktoru a pravdepodobnosti zriedkavého kaónového rozpadu $K^+ \to \pi^+\mu^+\mu^-$ ($K_{\pi\mu\mu}$) na NA62 experimente, použitím časti dát z roku 2017. Z tohoto dôvodu práca opisuje motiváciu merania, zhŕňa teoretický opis v rámci chirálnej poruchovej teórie a vymenúva predchádzajúce merania parametrov rozpadu $K_{\pi\mu\mu}$.

Centrálnou časťou práce je detailný opis $K_{\pi\mu\mu}$ analýzy vykonanej autorom, ako aj odvodenie a validovanie fitovacej procedúry použitej na získanie parametrov form faktoru rozpadu $K_{\pi\mu\mu}$. Na základe vzorky 3074 kandidátov na rozpad $K_{\pi\mu\mu}$, pozorovaných v analyzovanej vzorke dát z roku 2017, sme zmerali hodnoty parametrov form-faktoru $a = -0.564 \pm 0.042$ a $b = -0.797 \pm 0.164$, čo dáva hodnotu modelovo závislej pravdepodobnosti rozpadu $\mathcal{B}(K_{\pi\mu\mu}) = (9.32 \pm 0.29) \times 10^{-8}$. Dosiahnuté výsledky sú v zhode s predchádzajúcimi meraniami.

Vďaka nízkej kontaminácii vybranej vzorky pozaďovými rozpadmi sú výsledné štatistické chyby o $\approx$ 10–20% menšie v porovnaní s doteraz najpresnejším meraním $K_{\pi\mu\mu}$ rozpadu vykonaného experimentom NA48/2 na približne rovnako veľkej vzorke $K_{\pi\mu\mu}$ rozpadov, avšak s $\approx$ 3% pozaďových eventov.

Odhad systematických neistôt v našej analýze je však na úrovni štatistických chýb, čo robí výslednú presnosť nášho výsledku o $\approx$ 10–20% horšiu ako v prípade NA48/2. Zníženie systematických chýb je kľúčovým predpokladom na dosiahnutie svetovo významného výsledku, najmä po analyzovaní celého dostupného NA62 datasetu. Očakávaný počet signánlych eventov je aspoň 5-krát väčší ako počet $K_{\pi\mu\mu}$ rozpadov zaznamenaných na NA48/2.

Okrem analýzy $K_{\pi\mu\mu}$ rozpadu autor uskutočnil merania efektivít sub-detektorov MUV3 a CHOD, výsledky ktorých sú taktiež opísané v práci. Efektivity merané vyvinutými nástrojmi boli monitorované počas zberu dát v rokoch 2016–2018. Ich hodnoty sú stabilné a vyššie ako 99%. Výsledky merania efektivity MUV3 sú tiež použité v hlavnej analýze parametrov rozpadu $K_{\pi\mu\mu}$.

Hlavným cieľom NA62 experimentu je meranie tzv. ultra-zriedkavého rozpadu $K^+ \to \pi^+\nu\bar{\nu}$ ($K_{\pi\nu\nu}$), niekedy označovaného za "zlatý rozpad" kvôli čistote jeho teoretickej predpovede a cistlivosti na novú fyziku. Tieto vlastnosti robia rozpad $K_{\pi\nu\nu}$ výborným kandidátom na hľadanie fyziky za Štandardným Modelom. Predložená dizertačná práca opisuje meranie rozpadu $K_{\pi\nu\nu}$ a uvádza výsledky $K_{\pi\nu\nu}$ analýzy vykonanej na dátach zozbieraných v roku 2016.

Kľúčové slová: NA62 experiment, Zriedkavé rozpady kaónov, Form-faktor nabitého kaónu

1 Kaon Decay Physics

1.1 $K^+ \to \pi^+ \nu\bar{\nu}$ Decay

The NA62 experiment focuses on measurements of rare positive kaon decays, mainly the very-rare semileptonic decay $K^+ \to \pi^+ \nu\bar{\nu}$ with the theoretical prediction on the branching fraction [1]

$$\mathcal{B}(K^+ \to \pi^+ \nu\bar{\nu})_{\mathrm{SM}} = (8.4 \pm 1.0) \times 10^{-11} \ . \tag{1.1}$$

The best measurement of the $K^+ \to \pi^+ \nu\bar{\nu}$ branching fraction to date was done by the *stopped-kaon* experiments E787 and E949 at the Brookhaven National Laboratory[1] [2] and reads

$$\mathcal{B}(K^+ \to \pi^+ \nu\bar{\nu})_{\mathrm{Exp}} = (17.3^{+11.5}_{-10.5}) \times 10^{-11} \ . \tag{1.2}$$

This result comes from the total number of *seven* $K^+ \to \pi^+ \nu\bar{\nu}$ decay candidates, as is shown in Fig. 1.1.

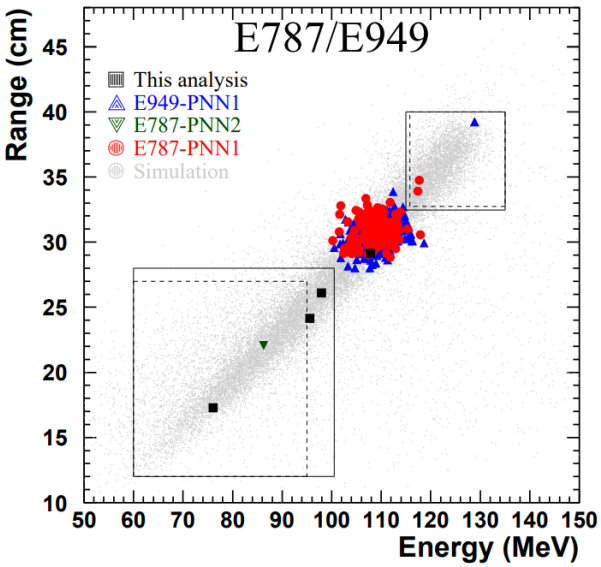

Figure 1.1: The seven $K^+ \to \pi^+ \nu\bar{\nu}$ signal events selected by the E787 and E949 analyses. The solid and dashed lines define signal regions. See [2] for more details.

In Table 1.1, we show a list of the most relevant charged kaon decays together with their branching fractions.

[1] https://www.bnl.gov/world/

Decay mode	Abbreviation	Type	Branching fraction ($\mathcal{B}$)
$K^+ \to \mu^+\nu_\mu$	$K_{\mu 2}$	leptonic	$(63.56 \pm 0.11)\%$
$K^+ \to \pi^+\pi^0$	$K_{2\pi}$	hadronic	$(20.67 \pm 0.08)\%$
$K^+ \to \pi^+\pi^+\pi^-$	$K_{3\pi}$	hadronic	$(5.583 \pm 0.024)\%$
$K^+ \to \pi^0 e^+\nu_e$	K_{e3}	semileptonic	$(5.07 \pm 0.04)\%$
$K^+ \to \pi^0\mu^+\nu_\mu$	$K_{\mu 3}$	semileptonic	$(3.352 \pm 0.033)\%$
$K^+ \to \pi^+\pi^- e^+\nu_e$	K_{e4}	semileptonic	$(4.247 \pm 0.024) \times 10^{-5}$
$K^+ \to \pi^+\pi^-\mu^+\nu_\mu$	$K_{\mu 4}$	semileptonic	$(1.4 \pm 0.9) \times 10^{-5}$
$K^+ \to \pi^+ e^+ e^-$	$K_{\pi ee}$	semileptonic	$(3.00 \pm 0.09) \times 10^{-7}$
$K^+ \to \pi^+\mu^+\mu^-$	$K_{\pi\mu\mu}$	semileptonic	$(9.4 \pm 0.6) \times 10^{-8}$
$K^+ \to e^+\nu_e e^+ e^-$	$K_{e\nu ee}$	leptonic	$(2.48 \pm 0.20) \times 10^{-8}$
$K^+ \to \mu^+\nu_\mu\mu^+\mu^-$	$K_{\mu\nu\mu\mu}$	leptonic	$< 4.1 \times 10^{-7}$ at 90% CL
$K^+ \to \pi^+\nu\bar{\nu}$	$K_{\pi\nu\nu}$	semileptonic	$(1.7 \pm 1.1) \times 10^{-10}$

Table 1.1: Positive kaon decays relevant for this thesis and their measured branching fractions, [3].

1.2 $K \to \pi l^+ l^-$ Decays

In light of tensions between the Standard Model predictions and experimental measurements in the B-physics sector [4, 5], investigations of possibilities to probe lepton flavour universality violation (LFUV) and lepton flavour violation (LFV) at NA62 and other kaon experiments have been carried out in [6]. Charged kaon decays $K^\pm \to \pi^\pm l^+ l^-$ are mentioned as examples of LFUV tests. The main analysis of the presented thesis is the measurement of the $K^+ \to \pi^+\mu^+\mu^-$ ($K_{\pi\mu\mu}$) decay form factor and branching fraction.

An extensive work [7, 8, 9, 10, 11] has been done towards theoretical understanding of $K^\pm \to \pi^\pm l^+ l^-$ decays, mainly their dominant contributions mediated by one virtual photon exchange $K^\pm \to \pi^\pm\gamma^* \to \pi^\pm l^+ l^-$ and involving long-distance hadronic effects. As these effects are difficult to describe, the calculations were done in the scope of the Chiral Perturbation Theory (ChPT) up to the next-to-leading order (NLO) [9] as well as in the combined framework of the ChPT and the Large-N_c QCD [10]. More recent attempts of lattice QCD calculations of $K^\pm \to \pi^\pm l^+ l^-$ amplitudes [12] are still operating with unphysical meson masses.

Since the presented thesis is focused on the muonic decay mode $K^+ \to \pi^+\mu^+\mu^-$ ($K_{\pi\mu\mu}$), from now on we substitute muons in place of the out-going leptons in $K^\pm \to \pi^\pm l^+ l^-$. Assuming LFU, all relations hold also for the electron mode as long as proper lepton mass is used.

At low energies, the $K_{\pi\mu\mu}$ decay is described by an effective theory derived in [7, 9]. The dominant long-distance contribution to the $K_{\pi\mu\mu}$ decay, originating from the radiative transition $K^+ \to \pi^+\gamma^*$, is very well described by the effective lagrangian of the ChPT [7]. The amplitude of the transition $K^+ \to \pi^+\gamma^*$ vanishes at tree-level [7] and the first

non-zero contribution to this process comes from one-loop diagrams.

Let us denote the momenta of the particles involved in the $K^+ \to \pi^+\mu^+\mu^-$ decay as

$$K^+(k) \to \pi^+(p)\mu^+(q_+)\mu^-(q_-)\ . \tag{1.3}$$

Combining the one-loop contributions from the lowest-order effective chiral lagrangian with tree-level contributions from the 4-th order lagrangian, a final decay amplitude is obtained, shown here using conventions listed in [9]

$$A\left(K^+(k) \to \pi^+(p)\mu^+(q_+)\mu^-(q_-)\right) = -\frac{e^2}{M_K^2(4\pi)^2}W(z)(k+p)^\mu \bar{u}(q_-)\gamma_\mu v(q_+), \tag{1.4}$$

where $k^2 = M_K^2$, $p^2 = m_\pi^2$, $q = k - p = q_+ + q_-$, $z = q^2/M_K^2$, γ^μ are gamma matrices, u and v are fermionic fields corresponding to outgoing muons, and $W(z)$ is a form factor describing dynamics of the decay (see Eq. 1.8).

Finally, the differential decay width in terms of the di-muon invariant mass is[2]

$$\frac{\mathrm{d}\Gamma_0}{\mathrm{d}z} = \frac{\alpha^2 M_K}{12\pi(4\pi)^4}\lambda^{3/2}(1, z, r_\pi^2)\sqrt{1 - 4\frac{r_\mu^2}{z}}\left(1 + 2\frac{r_\mu^2}{z}\right)|W(z)|^2, \tag{1.5}$$

with $r_i = m_i/M_K$, $\lambda(a,b,c) = a^2 + b^2 + c^2 - 2(ab + ac + bc)$ and $4r_\mu^2 \leq z \leq (1 - r_\pi)^2$.

The decay width shown in Eq. 1.5 is corrected for long-distance Coulomb interactions using functions $\Omega_{\mathrm{C}}(s_{ij})$ [13]

$$\frac{\mathrm{d}^2\Gamma}{\mathrm{d}x\mathrm{d}z} \equiv \frac{\mathrm{d}^2\Gamma_0}{\mathrm{d}x\mathrm{d}z} \times \frac{\mathrm{d}^2\Gamma_{\mathrm{Coulomb}}}{\mathrm{d}x\mathrm{d}z} = \frac{\mathrm{d}^2\Gamma_0}{\mathrm{d}x\mathrm{d}z} \times \Omega_{\mathrm{C}}(s_{\pi^+\mu^+}) \times \Omega_{\mathrm{C}}(s_{\pi^+\mu^-}) \times \Omega_{\mathrm{C}}(s_{\mu^+\mu^-}), \tag{1.6}$$

where $x = M(\pi^+, \mu^+)/M_K^2$, $s_{ij} = (p_i + p_j)^2$ and $(ij) \in \{\pi^+\mu^+, \pi^+\mu^-, \mu^+\mu^-\}$. The Coulomb term for each particle pair (ij) in the final state is defined as

$$\Omega_{\mathrm{C}}(s_{ij}) = \frac{2\pi\alpha Q_i Q_j}{\beta_{ij}(s_{ij})} \times \left[e^{\frac{2\pi\alpha Q_i Q_j}{\beta_{ij}(s_{ij})}} - 1\right]^{-1}, \quad \beta_{ij}(s_{ij}) = \left[1 - \frac{4m_i^2 m_j^2}{(s_{ij} - m_i^2 - m_j^2)^2}\right]^{1/2}. \tag{1.7}$$

The effect of Coulomb corrections is shown in Fig. 1.2. The plots are obtained using the form factor $W(z)$ parameters set to the values measured by the NA48/2 experiment [14]. For this particular choice of the form factor parameter values, the Coulomb corrections amount to $\approx 3\%$ increase in the total $K_{\pi\mu\mu}$ branching fraction.

For the purposes of our analysis, we chose the $K_{\pi\mu\mu}$ form factor parametrisation in the scope of the ChPT

$$W(z) = G_F M_K^2(a + bz) + W^{\pi\pi}(z), \tag{1.8}$$

[2]The "0" in the subscript of the differential decay width $\mathrm{d}\Gamma_0/\mathrm{d}z$ is meant to indicate that the Coulomb corrections have not been applied yet.

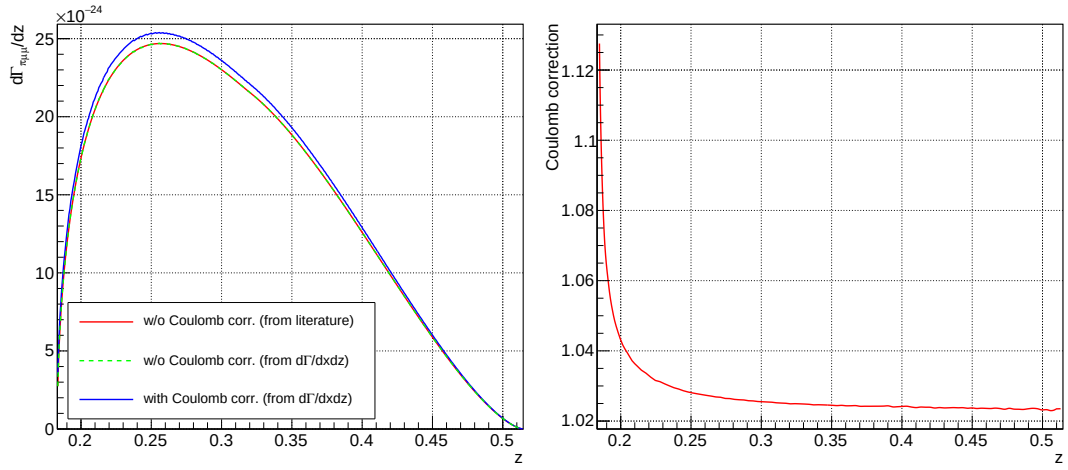

Figure 1.2: Left: $K_{\pi\mu\mu}$ differential decay width $\mathrm{d}\Gamma/\mathrm{d}z$ with and without Coulomb corrections. Green line is meant as a sanity check: it represents our numerically integrated 2D decay width $\mathrm{d}^2\Gamma/\mathrm{d}x\mathrm{d}z$ along x when no Coulomb corrections are applied. It is identical to the red line, which is a plot of formula 1.5, found for example in [9]. Right: $\mathrm{d}^2\Gamma_{\mathrm{Coulomb}}/\mathrm{d}z$ computed as a ratio of the blue and green curves in the left plot. The correction diverges in the limit of low z, which corresponds to zero relative velocity of the muon pair.

with the pion loop term $W^{\pi\pi}(z)$, arising from contributions of $K^+ \to \pi^+\pi^+\pi^-$ with $\pi^+\pi^- \to \gamma^*$ rescattering [9].

The main analysis of the presented thesis can be regarded as a preliminary measurement of the $K_{\pi\mu\mu}$ form factor parameters by the NA62 experiment. Once the full dataset collected in 2017 and 2018 is analysed, the cumulative $K_{\pi\mu\mu}$ sample should be the largest one in the world. If the final systematic errors can be held reasonably low, the NA62 has a potential to challenge the LFU or at least improve the previous measurements [14, 15, 16].

2 Measurement of $K^+ \to \pi^+\mu^+\mu^-$ Decay Form Factor

2.1 Analysis Summary

The main goal of the NA62 experiment, a measurement of the $K^+ \to \pi^+\nu\bar{\nu}$ decay branching fraction, requires a high intensity kaon beam and a detector setup comprising precise particle tracking and timing, and high-efficiency particle identification and photon detection. This allows for studies of other rare processes to be performed at NA62 in parallel to the main decay mode analysis.

One of the most interesting kaon decay channels is the semileptonic decay $K^+ \to \pi^+\mu^+\mu^-$ ($K_{\pi\mu\mu}$), theoretically described in section 1.2. An analysis of the $K_{\pi\mu\mu}$ decay with a measurement of the form factor parameters a and b (see Eq. 1.8) is the main goal of the presented thesis.

A measurement of both form factor parameters is equivalent to the simultaneous determination of the overall scale and shape of the differential decay width (Eq. 1.6 and Eq. 1.8). This implies that the obtained sample of $K_{\pi\mu\mu}$ decays needs to be properly normalised using another K^+ decay channel. The $K^+ \to \pi^+\pi^+\pi^-$ ($K_{3\pi}$) decay was selected as the normalisation in our analysis for two main reasons.

Firstly, the $K_{3\pi}$ decay is abundant (see Table 1.1), which allows for the collection of a large $K_{3\pi}$ sample, practically eliminating the systematic error on $K_{\pi\mu\mu}$ form factor parameters arising from the normalisation.

Secondly, the $K_{3\pi}$ decay is kinematically similar to the $K_{\pi\mu\mu}$ decay — it contains three charged tracks originating from a common vertex and no other particles in the final state, which allows for minimal differences in the corresponding event selection procedures, thus reducing both the complexity of the analysis as well as various possible systematic effects.

Due to the similarity between the signal and the normalisation channels and relatively small branching fractions of other three-track decay modes, the $K_{3\pi}$ decay channel is also the most important potential source of the background in the selected $K_{\pi\mu\mu}$ sample. Therefore, the particle identification (PID) and a small difference in decay kinematics play a crucial role in the suppression of the $K_{3\pi}$ background. The NA62 beam and sub-detectors used in our analysis are described in [17].

In order to determine acceptances of the developed $K_{\pi\mu\mu}$ signal and $K_{3\pi}$ normalisation event selections, we used simulated Monte Carlo (MC) samples of $K_{\pi\mu\mu}$ and $K_{3\pi}$ decays.

The results are

$$A(K_{3\pi}) = (10.14 \pm 0.01_{\text{stat}})\%, \qquad A(K_{\pi\mu\mu}) = (12.77 \pm 0.02_{\text{stat}})\% \ . \tag{2.1}$$

The data sample employed in this analysis was recorded in September and October 2017 with relatively stable data taking conditions. The used dataset constitutes

$$N_{\text{K}} = (5.17 \pm 0.01_{\text{stat}} \pm 0.43_{\text{syst}}) \times 10^{11} \tag{2.2}$$

kaon decays. N_{K} was measured from data events passing our $K_{3\pi}$ event selection with the selection acceptance obtained from the $K_{3\pi}$ MC sample described above. The regions marked by black arrows in Fig. 2.1 contain

$$N(K_{3\pi}) \approx 2.93 \times 10^7, \qquad N(K_{\pi\mu\mu}) = 3074 \tag{2.3}$$

events in data.

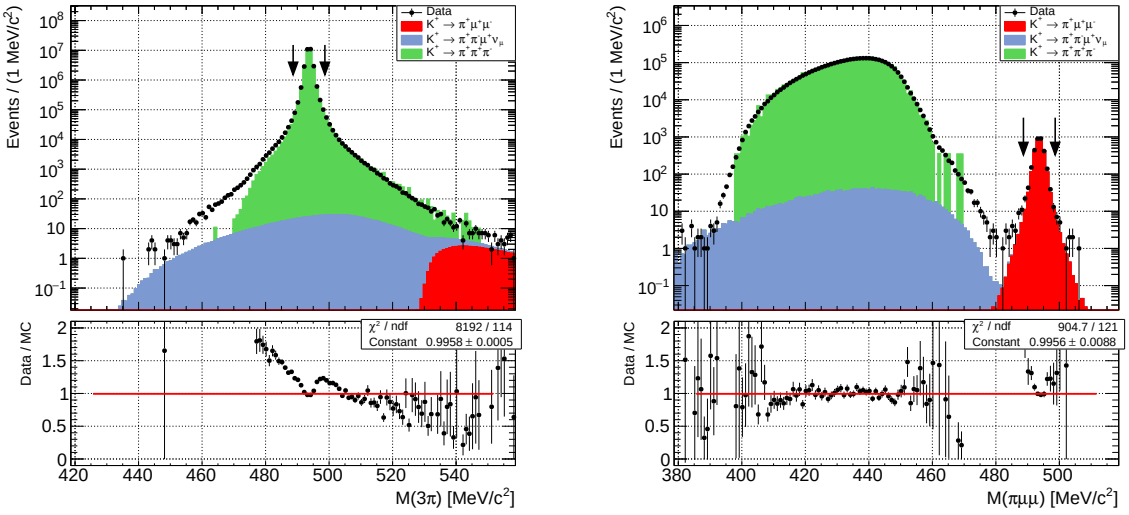

Figure 2.1: $M(3\pi)$ ($M(\pi\mu\mu)$) invariant mass spectrum is showed on the left (right). Arrows indicate signal regions. The bulk of events to the left of the signal peak in the $M(\pi\mu\mu)$ spectrum are predominantly $K_{3\pi}$ decays with two $\pi \to \mu\nu$ decays, denoted as $K_{3\pi} \to 2\mu$ in the following text.

In our analysis, we used specialised tools to inject accidental hits into pure reconstructed MC events containing one single kaon decay. This was done in order to emulate the pileup observed in data, caused either by decays of other particles present in the high-intensity NA62 beam or by the presence of a muon halo accompanying the beam. The author developed a tool for injecting accidentals into the MUV3 sub-detector, used for PID in the $K_{\pi\mu\mu}$ event selection. The tool is described in section 2.2.

The $K_{\pi\mu\mu}$ signal and $K_{3\pi}$ normalisation data samples were collected using separate trigger streams, called Di-muon and Multi-track, respectively. Measurements of the underlying

trigger efficiencies play crucial role in our analysis since they affect both shape and scale of the resulting $K_{\pi\mu\mu}$ z spectrum (Eq. 1.5).

In the case of the Multi-track trigger stream used for collecting the $K_{3\pi}$ normalisation channel, it was possible to measure the corresponding trigger efficiencies directly from data. However, due to the limited number of observed $K_{\pi\mu\mu}$ decays in data and non-existence of another non-rare K^+ decay mode producing a muon pair, it was impossible to reliably measure the trigger efficiency of the Di-muon trigger stream used for collecting the $K_{\pi\mu\mu}$ signal events. Therefore, detailed L0 and simplified L1 trigger emulators were developed, tuned and applied on MC samples on an event-by-event basis, using the accept/reject method. We show the total measured and emulated trigger efficiencies in Table 2.1.

Sample	$K_{3\pi}$		$K_{3\pi} \to 2\mu$		$K_{\pi\mu\mu}$
Type	Measured	Emulated	Measured	Emulated	Emulated
$1-\varepsilon$(RICH)	0.023(1)	0.001(1)	0.054(29)	0.001(1)	0.001(1)
$1-\varepsilon$(QX)	1.631(6)	1.685(6)	1.486(117)	1.747(136)	1.224(10)
$1-\varepsilon$(MO2 | QX)	–	–	0.020(9)	0.076(37)	0.089(3)
$1-\varepsilon$(KTAG)	0.166(5)	0.163(2)	–	–	–
$1-\varepsilon$(STRAW$_e$)	4.375(26)	4.740(10)	3.988(74)	4.606(212)	4.025(18)
Total inefficiency	6.112(27)	6.499(12)	5.485(137)	6.345(248)	5.285(20)

Table 2.1: Measured and emulated trigger inefficiencies (in %) of Multi-track and Di-muon trigger components. The quoted errors are statistical only.

The $K_{\pi\mu\mu}$ z spectrum (Fig. 2.2) obtained from the $K_{\pi\mu\mu}$ data candidates is compared to the z spectrum of *weighted* MC events. The reweighting of the MC z spectrum is done event-by-event using the weight function

$$w_i(a,b) = \frac{\mathrm{d}\Gamma({z^{\mathrm{truth}}_{\mathrm{MC}}}_i, a, b)}{\mathrm{d}\Gamma({z^{\mathrm{truth}}_{\mathrm{MC}}}_i, a_{\mathrm{NA62\ MC}}, b_{\mathrm{NA62\ MC}})}, \tag{2.4}$$

where ${z^{\mathrm{truth}}_{\mathrm{MC}}}_i$ is the true value of z for i-th $K_{\pi\mu\mu}$ MC event passing our $K_{\pi\mu\mu}$ event selection. The fitted form factor parameters a and b are determined based on the best agreement between the data and the weighted MC z spectra. The total $K_{\pi\mu\mu}$ branching fraction is computed by numerical integration of the Coulomb-corrected $\mathrm{d}^2\Gamma/\mathrm{d}x\mathrm{d}z$ function shown in Eq. 1.6.

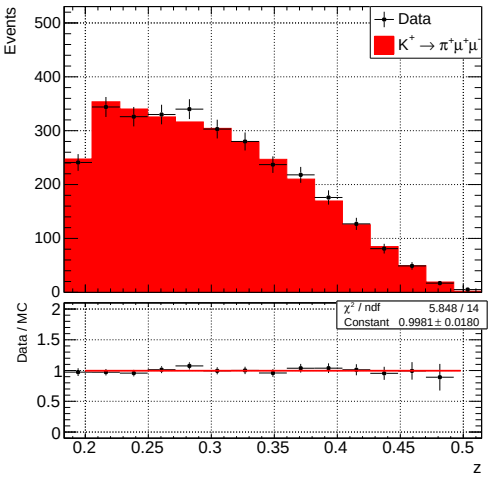

Figure 2.2: z spectrum of events passing our $K_{\pi\mu\mu}$ event selection shown here *before fitting*. The exceptionally good agreement between data and MC z spectra suggests the values of $K_{\pi\mu\mu}$ form factor parameters used in the NA62 MC generator should not be far from the ones obtained after the fitting procedure.

The measured form factor parameters are

$$\begin{aligned} a &= -0.564 \pm 0.034_{\text{stat}} \pm 0.024_{\text{syst}} \pm 0.001_{\text{ext}} = -0.564 \pm 0.042, \\ b &= -0.797 \pm 0.118_{\text{stat}} \pm 0.114_{\text{syst}} \pm 0.003_{\text{ext}} = -0.797 \pm 0.164, \end{aligned} \tag{2.5}$$

which gives the model-dependent $K_{\pi\mu\mu}$ branching fraction equal to

$$\mathcal{B}(K_{\pi\mu\mu}) \times 10^8 = 9.32 \pm 0.17_{\text{stat}} \pm 0.23_{\text{syst}} \pm 0.04_{\text{ext}} = 9.32 \pm 0.29\ . \tag{2.6}$$

In Fig. 2.3, we show comparison of the $K_{\pi\mu\mu}$ form factor parameters a and b obtained in this analysis and in the previous experiments E865 [16] and NA48/2 [14, 15].

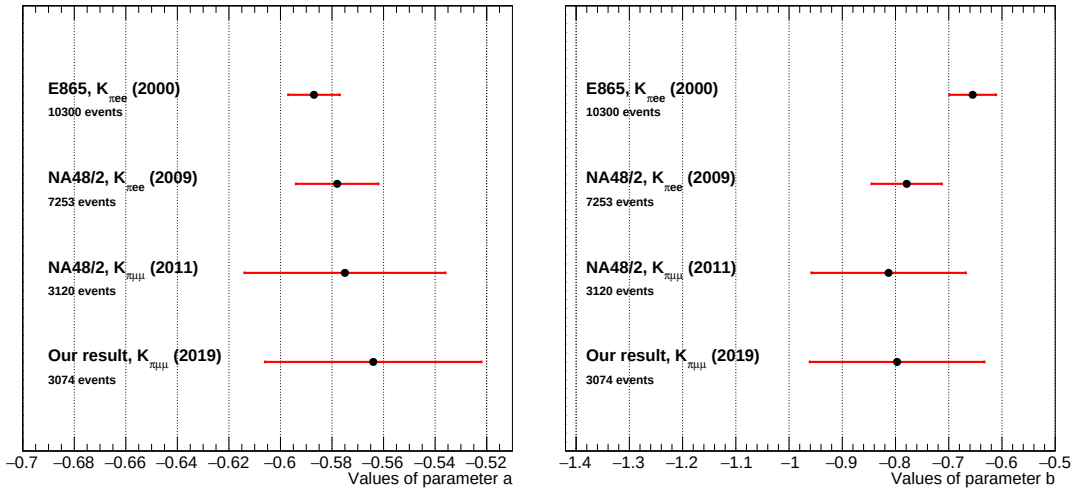

Figure 2.3: Comparison of world data on $K^\pm \to \pi^\pm l^+ l^-$ form factor parameters.

2.2 MUV3 Pileup Generator

Due to the fact that the NA62 is a high-intensity experiment, the high rates of hits in individual sub-detectors generally result in accidental inclusion of signals from different (kaon) decays or from halo muons in a single event. This fact has an impact on track reconstruction, PID, trigger efficiency, etc.

Since individual MC events are generated such that one event corresponds to an isolated kaon decay, no pileup hits are present in sub-detectors by default. If this fact was not accounted for, it would result in differences between simulated and real detector performance. We therefore use multiple pileup generators designed to inject pileup into MC events.

One such tool is a MUV3 pileup generator developed by the author of the presented thesis. It injects accidental hits and candidates to MUV3 MC event based on distributions obtained from data. Minimum-bias data is used for acquiring these distributions.

The tool is initially run over the analysed dataset in order to determine the spatial distribution and the number of accidental muons registered out-of-time from the trigger in order to avoid counting muons from triggered kaon decays. Both distributions are shown in Fig. 2.4.

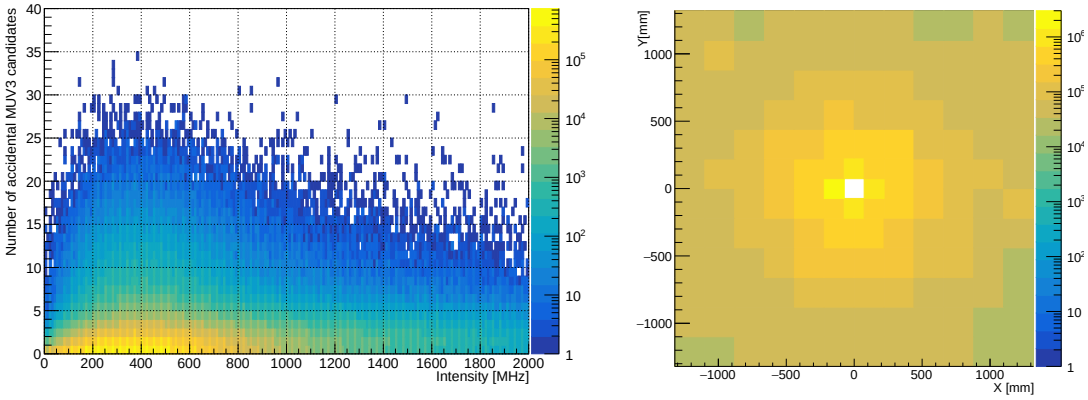

Figure 2.4: Left: the number of accidental MUV3 candidates versus instantaneous beam intensity as measured from data. Right: spatial distribution of accidental MUV3 candidates in data (arbitrary units).

The first step in the algorithm generating the number of accidentals for a particular MC event is a request of the value of the instantaneous beam intensity, chosen randomly by a separate tool. Subsequently, the number of accidental candidates is determined by sampling the corresponding slice of the two-dimensional histogram shown in Fig. 2.4 (left). Tile ID, determining position of each accidental candidate, is chosen randomly according to the hit-map shown in Fig. 2.4 (right). The injected accidental (pileup) hits and candidates are then treated as "real" MUV3 hits/candidates in our $K_{\pi\mu\mu}$ analysis.

3 MUV3 and CHOD Efficiency Studies

In order to ensure high quality of the collected data necessary for a successful fulfilment of the NA62 physics plan, several online and offline tools have been developed by members of the Collaboration to monitor the data taking.

Author of the presented thesis developed tools for offline monitoring of the efficiency of MUV3 and CHOD sub-detectors. The following sections describe these tools and show examples of their outputs obtained on Monte Carlo simulation (MC) and minimum-bias data sample corresponding to 2017 runs used in the main analysis of the presented thesis.

3.1 MUV3 Efficiency Measurement

The basic principle of the MUV3 efficiency tool involves extrapolation of Straw tracks identified as muons by RICH, LKr, MUV1 and MUV2 sub-detectors to the MUV3 plane and checking if a reconstructed MUV3 candidate compatible in both time and space is present in the event.

A combination of two different samples for measuring MUV3 efficiency is used by default: halo muons accompanying the hadron beam, and muons from $K^+ \to \mu^+\nu_\mu$ decays (see Table 1.1). One of the advantages of using both samples is the fact that the muon halo, consisting of both positive and negative muons, covers almost full MUV3 acceptance. This is not true for muons produced in the $K_{\mu 2}$ decays which, due to their positive charge, are swept in the negative-X direction by the Straw magnet and completely miss some MUV3 tiles.

The choice between the halo and $K_{\mu 2}$ selections is done automatically on an event-by-event basis, creating a combined muon sample on which the MUV3 efficiency is estimated.

The main goal of the event selection is to select a well-reconstructed muon track without using the MUV3 sub-detector. The particle identification is therefore performed using only MUV1, MUV2, LKr and RICH sub-detectors.

This track identified as a muon is then extrapolated to the MUV3 front-plane and a check for compatible reconstructed muon candidate in MUV3 is performed.

The MUV3 efficiency measurement tool outputs a list of bursts with the total efficiency lower than a predefined threshold, set to 96% by default. This list is then used in user analyses to automatically skip MUV3-inefficient bursts. The measured efficiency plots in the form of a `pdf` file are also created, which helps in visualisation of the measured quantities.

Figure 3.1 (left) displays how the efficiency measured on data depends on the muon

momentum. The total MUV3 efficiency measured in the analysed data sample is

$$\varepsilon(\text{MUV3, data, full } p \text{ range}) = (99.701 \pm 0.001_{\text{stat}} \pm 0.027_{\text{syst}})\,\%, \tag{3.1}$$

where the systematic error was estimated as a difference between the results obtained when the tool is forced to measure the efficiency only on $K_{\mu 2}$ or halo muons.

We also computed the total MUV3 efficiency for track momenta below 60 GeV/c, which is a limit of the momenta of $K_{\pi\mu\mu}$ decay products. The total MUV3 efficiency in this momentum range was measured to be

$$\varepsilon(\text{MUV3, data, } p \text{ below 60 GeV}/c) = (99.813 \pm 0.001_{\text{stat}} \pm 0.002_{\text{syst}})\,\%, \tag{3.2}$$

with the efficiency increase with respect to Eq. 3.1 caused by discarding the inefficient events with tracks extrapolated to inner MUV3 tiles and track momenta around 75 GeV/c (see Fig. 3.1 (left)).

To test whether the measured MUV3 efficiency in MC is close to unity, the presented tool has also been run on an official $K_{\mu 2}$ MC sample with the total efficiency

$$\varepsilon(\text{MUV3, MC, } p \text{ below 60 GeV}/c) = (99.953 \pm 0.001_{\text{stat}})\,\% \ . \tag{3.3}$$

Muon momentum efficiency dependence for $K_{\mu 2}$ MC events is shown inFig. 3.1 (right).

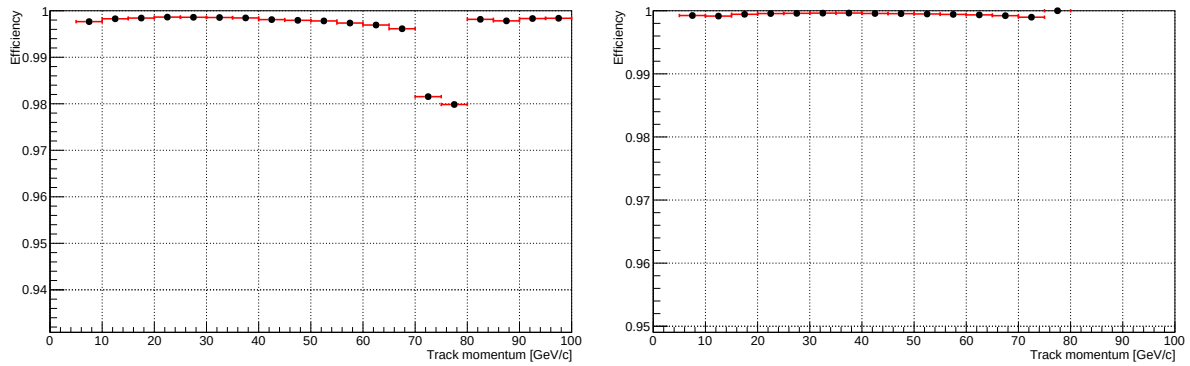

Figure 3.1: MUV3 efficiency as a function of muon momentum from data (left) and $K_{\mu 2}$ MC (right). Clearly visible efficiency drop can be seen around 75 GeV/c in data originating from beam pions close to the beam pipe that are extrapolated to the MUV3 acceptance but in reality miss the MUV3, thus creating an artificial inefficiency.

The above results from Eq. 3.2 and Eq. 3.3 are used in the $K^+ \to \pi^+\mu^+\mu^-$ decay form factor measurement to emulate MUV3 sub-detector inefficiency on MC samples.

3.2 CHOD Efficiency Measurement

The tool used for CHOD efficiency measurement is also based on track-seeded checks for the presence of a compatible CHOD candidate.

Since the MUV3 and CHOD sub-detectors have a similar design involving scintillator tiles, the tool used for the CHOD efficiency measurement was derived from the one used for the MUV3 efficiency evaluation.

However, since the CHOD should see all charged particles in its acceptance, no particle identification has to be made, which makes the CHOD tool significantly simpler.

The tool produces a list of inefficient ("bad") bursts which can then be skipped later at the analysis stage. A burst is defined as bad by the CHOD efficiency tool if the overall burst efficiency integrated over all CHOD tiles drops below 96%.

As in the case of the MUV3 efficiency tool, the CHOD efficiency tool also exports the measured efficiency spectra in the form of a `pdf` file which helps visualising possible inefficiencies. An example of the output obtained from a minimum-bias data sample is shown in Fig. 3.2.

The overall CHOD efficiency is

$$\varepsilon(\text{CHOD, data}) = (99.459 \pm 0.001_{\text{stat}})\,\%. \tag{3.4}$$

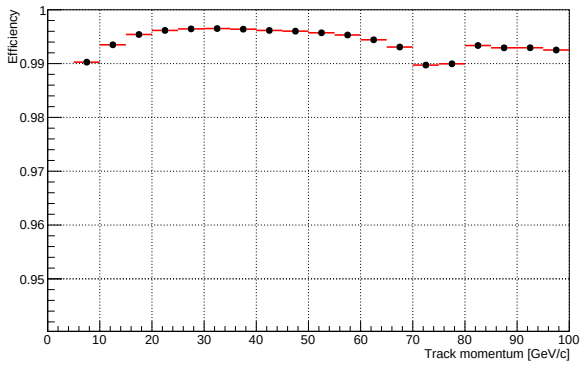

Figure 3.2: CHOD efficiency as a function of muon momentum, integrated over all tiles. The drop in the efficiency at 75 GeV/c momentum is caused by the beam particles passing the selection cuts but missing the actual CHOD acceptance. Similarly, the decrease in efficiency for low momenta is mostly caused by the track extrapolating to outer CHOD tiles, but in reality missing the CHOD acceptance.

Bibliography

[1] A. J. Buras, D. Buttazzo, J. Girrbach-Noe, and R. Knegjens, *$K^+ \to \pi^+\nu\nu$ and $K_L \to \pi^0\nu\nu$ in the standard model: status and perspectives*, Journal of High Energy Physics, 2015 (2015), p. 33.

[2] A. V. Artamonov et al., *Study of the decay $K^+ \to \pi^+\nu\bar{\nu}$ in the momentum region $140 < P_\pi < 199$ MeV/c*, Phys. Rev., D79 (2009), p. 092004, 0903.0030.

[3] M. Tanabashi et al., *Review of particle physics*, Phys. Rev. D, 98 (2018), p. 030001.

[4] R. Aaij et al., *Test of lepton universality using $B^+ \to K^+\ell^+\ell^-$ decays*, Phys. Rev. Lett., 113 (2014), p. 151601, 1406.6482.

[5] R. Aaij et al., *Measurement of the ratio of branching fractions $\mathcal{B}(\bar{b}^0 \to D^{*+}\tau^-\overline{\nu}_\tau)/\mathcal{B}(\bar{b}^0 \to D^{*+}\mu^-\overline{\nu}_\mu)$*, Phys. Rev. Lett., 115 (2015), p. 111803.

[6] L. C. Tunstall, A. Crivellin, G. D'Ambrosio, and M. Hoferichter, *Probing lepton flavour (universality) violation at NA62 and future kaon experiments*, J. Phys. Conf. Ser., 800 (2017), p. 012014, 1611.00495.

[7] G. Ecker, A. Pich, and E. de Rafael, *$K \to \pi l^+ l^-$ Decays in the Effective Chiral Lagrangian of the Standard Model*, Nucl. Phys., B291 (1987), p. 692.

[8] G. D'Ambrosio, G. Ecker, G. Isidori, and H. Neufeld, *Radiative nonleptonic kaon decays*, in 2nd DAPHNE Physics Handbook:265-313, 1994, pp. 265–313, hep-ph/9411439.

[9] G. D'Ambrosio, G. Ecker, G. Isidori, and J. Portoles, *The Decays $K \to \pi l^+ l^-$ beyond leading order in the chiral expansion*, JHEP, 08 (1998), p. 004, hep-ph/9808289.

[10] S. Friot, D. Greynat, and E. De Rafael, *Rare kaon decays revisited*, Phys. Lett., B595 (2004), pp. 301–308, hep-ph/0404136.

[11] A. Z. Dubnickova, S. Dubnicka, E. Goudzovski, V. N. Pervushin, and M. Secansky, *Kaon decay probe of the weak static interaction*, Phys. Part. Nucl. Lett., 5 (2008), pp. 76–84, hep-ph/0611175.

[12] N. H. Christ, X. Feng, A. Juttner, A. Lawson, A. Portelli, and C. T. Sachrajda, *First exploratory calculation of the long-distance contributions to the rare kaon decays $K \to \pi\ell^+\ell^-$*, Phys. Rev., D94 (2016), p. 114516, 1608.07585.

[13] G. Isidori, *Soft-photon corrections in multi-body meson decays*, Eur. Phys. J., C53 (2008), pp. 567–571, 0709.2439.

[14] J. R. Batley et al., *New measurement of the $K^\pm \to \pi^\pm\mu^+\mu^-$ decay*, Phys. Lett., B697 (2011), pp. 107–115, 1011.4817.

[15] ——, *Precise measurement of the $K^\pm \to \pi^\pm e^+e^-$ decay*, Phys. Lett., B677 (2009), pp. 246–254, 0903.3130.

[16] R. Appel et al., *A New measurement of the properties of the rare decay $K^+ \to \pi^+e^+e^-$*, Phys. Rev. Lett., 83 (1999), pp. 4482–4485, hep-ex/9907045.

[17] E. Cortina Gil et al., *The beam and detector of the NA62 experiment at cern*, Journal of Instrumentation, 12 (2017), p. P05025.

Author's Publications

1. L. Bičian (on behalf of the NA62 Collaboration), *Search for heavy neutral lepton production in K^+ decays at NA62*, PoS (ALPS2018) 005.
2. L. Bičian (on behalf of the NA62 Collaboration), *Limits on heavy neutrinos at NA48/2 and NA62*, International Journal of Modern Physics: Conference Series, 46(1860043), 2018.
3. L. Bičian, *$K^+ \to \pi^+\mu^+\mu^-$ analysis on 2017 Sample A*, NA62 Internal Note, NA62-19-05, 2019.
4. Eduardo Cortina Gil et al. (NA62 Collaboration) *Search for heavy neutral lepton production in K^+ decays*, Physics Lett., B778: 137-145, 2018.
5. Eduardo Cortina Gil et al. (NA62 Collaboration) *The beam and detector of the NA62 experiment at CERN*, JINST, 12(05):P05025, 2017.
6. Eduardo Cortina Gil et al. (NA62 Collaboration) *First search for $K^+ \to \pi^+\nu\bar{\nu}$ using the decay-in-flight technique*, 1811.08508, 2018, *accepted to Phys. Lett. B.*